A Novel Ultrasonic Guided Wave-Based Method for Railway Contact Wire Defect Detection

Yong Chang, Nana Li, Jiyuan Zhao, Yu Wang, *Senior Member, IEEE*, and Zhe Yang

***Abstract*— Detection of defects in contact wire is significantly important to a railway system. Due to the insensitivity to the deep-seated defects, traditional optics-based methods fail to detect the internal defects of contact wire. To overcome this shortcoming, a new defect detection method based on ultrasonic guided wave is proposed in this article. Theoretical dispersion curves and wave structures for the TCG-110 contact wire are derived using a special modeling technique called the semi-analytical finite-element (SAFE) method. It is shown that the longitudinal-like $M3$ mode in the frequency range of 50–100 kHz is attractive for the proposed application. Then, the experimental scheme is established based on the pulse-echo configuration to detect the defects in contact wire. The echoes overlapping and drown problems in guided wave signal leading to the time resolution of original signal are too low to extract useful position information of defects. Hence, the sparse deconvolution method is introduced based on the convolution model of guided wave signal and sparse theory, and the time resolution of guided wave signal is significantly improved. The experimental results show that the proposed method can detect the defects in contact wire effectively with high accuracy.**

***Index Terms*— Contact wire, defect detection, sparse deconvolution, ultrasonic guided wave.**

I. Introduction

THE high-speed and reliability of high-speed railway proposed new requirements for the safety maintenance of a traction power supply system. Once the equipment in the traction supply system is put into use, it will be in service, and the service status of key equipment is directly related to the running performance of the train. As the only direct power source for high-speed railway, the contact wire has the characteristics of complex structure, outdoor erection without standby, and harsh service conditions. Meanwhile, the contact wire will inevitably suffer from insulation aging, mechanical damage, excessive temperature rises, and other performance changes in the working process [1], [2]. These characteristics make the contact wire more prone to failure than other equipment in the traction supply system [2]. Therefore, the good performance of contact wire is the basis to ensure the safe and stable operation of railway, an important part of a railway system.

With the development of computer technology and image-processing algorithm, it has become possible to use visual inspection technology to realize the structural health monitoring (SHM) of contact wire [3]. A contact wire wear measuring system was developed by The Technical University of Madrid [4], which used laser diodes as illumination source and linear charge coupled device (CCD) cameras to capture the reflected image to estimate the residual thickness of the contact wire. In [5], a data-driven support vector machine (SVM) model was developed to evaluate the contact wire status from huge amount of data, without requiring understanding the physical mechanism of the fault. A new contactless fault diagnosis approach for a pantograph–catenary system based on pattern recognition and image processing methods [6] was used to detect the position of a contact wire. Aydin *et al.* [7] presented a vision-based inspection system based on the firefly algorithm to detect the occurrence of arcing due to loss of contact wire. However, the common feature of the current detection device or system is that they are all based on optical methods [8], which are insensitive to the deep-seated defect. It is essential to develop a new detection method that can effectively overcome the drawback of optical technology.

As an effective method, ultrasonic guided wave has been widely used in the field of nondestructive testing (NDT) [9], [10] and SHM [11], [12]. Compared with bulk waves, guided wave has two obvious advantages. One is that the cross section of waveguide is completely covered during the propagation of guided wave, so that both the surface and internal defects of structure can be detected at the same time. The other is that the energy loss of guided wave is very small during the long-distance propagation, so the measurement of a large-area structure can be realized at a single transducer position. These advantages make guided wave inspection receive a great deal of attention in the past two decades. Some good and promising

Manuscript received February 14, 2022; revised April 25, 2022; accepted May 12, 2022. Date of publication May 27, 2022; date of current version June 8, 2022. This work was supported in part by the National Natural Science Foundation of China under Grant 51905151, in part by the National Natural Science Foundation of China under Grant 51975452, and in part by the High Level Talent Foundation of Henan University of Technology under Grant 2020BS022. The Associate Editor coordinating the review process was Dr. Datong Liu. *(Corresponding author: Jiyuan Zhao.)*

Yong Chang is with the School of Electromechanical Engineering and the Henan Key Laboratory of Super Hard Abrasive Grinding Equipment, Henan University of Technology, Zhengzhou 450001, China (e-mail: changyong@haut.edu.cn).

Nana Li is with the High-speed Transmission Division, Zhengzhou Research Institute of Mechanical Engineering, Zhengzhou 450052, China (e-mail: lnana89@163.com).

Jiyuan Zhao is with the Collaborative Innovation Center of High-End Manufacturing Equipment, Xi'an Jiaotong University, Xi'an 710049, China (e-mail: jiyuan.zhao@xjtu.edu.cn).

Yu Wang is with the School of Mechanical Engineering, Xi'an Jiaotong University, Xi'an 710049, China (e-mail: ywang95@xjtu.edu.cn).

Zhe Yang is with the School of Mechanical Engineering, Dongguan University of Technology, Dongguan 523808, China (e-mail: yangz@dgut.edu.cn).

Digital Object Identifier 10.1109/TIM.2022.3178492

results have been obtained with guided wave in inspection of metal plates [13], [14], a pipeline [15]–[18], a composite material structure [13], [19]–[22], and so on.

In this article, a new detection method for contact wire based on ultrasonic guided wave and sparse deconvolution is proposed for the high-precision detection of defects in contact wire. The proposed method consists of three steps. In step 1, the propagation characteristics of guided wave in contact wire are studied for the first time, and the semi-analytical finite-element (SAFE) method is employed to calculate the dispersion curves of contact wire. Meanwhile, the wave structures of different modes are compared and analyzed, which provides a theoretical basis for the future research of ultrasonic guided wave detection of contact wire. In step 2, the ultrasonic guided wave detection scheme of contact wire is studied to realize the effective detection of contact wire defects, which provides help for the engineering application of ultrasonic guided wave detection technology of contact wire. In step 3, the sparse deconvolution method is studied to solve the echoes overlapping and drown problems in original signals, and the high-precision detection of axial position of contact wire defect is realized. This work provides an effective and promising tool for contact wire defects detection.

In this article, an ultrasonic guided wave is used to detect the axial distance of contact wire defects with high precision, and the following specific questions are to be addressed.

1) The dispersive curves and wave structures of contact wire must be studied, because such information plays an important role in contact wire NDT that uses ultrasonic guided waves.
2) The time resolution of guided wave signal must be improved, because there are echoes overlapping and drown problems in original signals, leading to the time resolution is too low to extract the useful position information of defects directly.

The structure of this article is organized as follows. In Section I, the background introduction is given. The detailed theoretical studies on dispersive curves and wave structures are introduced in Section II. The effective experimental apparatus is studied in Section III. The sparse deconvolution method is introduced in Section IV. In Section V, the proposed method is applied to detect the defects in contact wire. The conclusions are given in Section VI.

II. Propagation Characteristics of Guided Wave in Contact Wire

A. Dispersion Curves of Contact Wire

To apply guided wave to contact wire, theoretical phase and group velocity dispersion curves of contact wire must be first obtained, because the dispersion curves present some essential information for guided waves, such as phase/group velocity at a certain frequency, wavelength, cutoff frequency, and energy attenuation. For example, to avoid generating signals that are too complicated to explain, it is essential to select a suitable mode and excitation frequency according to the cutoff frequency, energy attenuation, and dispersivity. The group velocity at excitation frequency is useful for extracting the travel times of wave signals, which are used to calculate the position of defect. Meanwhile, different group velocities can be used as characteristics to distinguish different models in the measured signals.

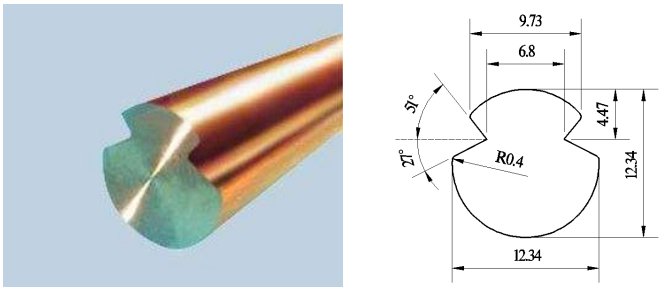

Fig. 1. Research object of this article TCG-110 contact wire. (a) Cross section. (b) Geometric size.

TABLE I
Material Properties of TCG-110 Contact Wire

Elastic Modulus (GPa)	Poisson's Ratio	Mass Density (Kg/m^3)
119	0.326	8890

Detailed investigations of dispersion curves for simple structures, such as hollow cylinders, plates, and rods, have been given by analytical methods. However, traditional methods fail to calculate dispersion curves of contact, because contact wire has an eight-shaped cross section, as shown in Fig. 1, which is more complex compared with simple structures. The SAFE method [23]–[26] was developed as an alternative approach to traditional analytical methods mainly because of its benefits of solving wave propagation problems of arbitrary cross-sectional waveguide. According to the theory of the SAFE method, the cross section of waveguide is subdivided into finite elements, and wave motions in the propagation direction are described by the orthogonal function. The theoretical analysis and calculation of the SAFE method have been discussed in detail in [23]–[26]; only the specific calculation process used in this article will be explained.

The TCG-110 type contact wire is considered in this article. The geometric size and material properties of TCG-110 contact wire are shown in Fig. 1 and Table I, respectively. According to the theory of the SAFE method, the specific calculation process of dispersion curves for TCG-110 contact wire is shown in Fig. 2.

As shown in Fig. 1, the cross section of contact wire has a complex geometry perpendicular to the axis of symmetry. In the finite-element model, the cross section of contact wire in the xy plane is divided into 587 nodes for 1083 triangular elements with linear interpolation displacement function. Wave displacement field in the longitudinal direction z is described by the orthogonal function $\exp(i\xi z)$, where ξ is the wavenumber of guided wave. The displacement vector over the element domain can be described as the shape functions and nodal displacements in the x-, y- and z-directions. Meanwhile, the strain vector in the element can be expressed as a function of nodal displacements. Then, the element kinetic energy

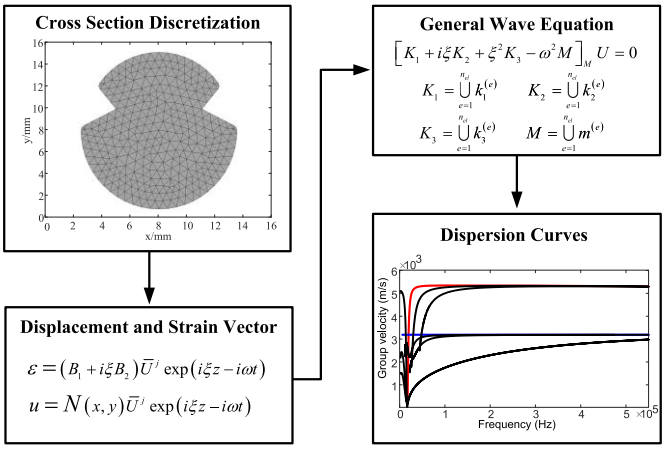

Fig. 2. Flow diagram for calculation of dispersion curves for TCG-110 contact wire using the SAFE method.

is given using the displacement vector and simplifying the harmonic terms, and the element strain energy is written as the strain vector. The equations of motion for the cross-sectional elements can be obtained by inserting the potential and kinetic energies into Hamilton's equation [23]–[26]. The discrete form of Hamilton's formulation is assembled by a standard finite-element assembling procedure, and the general governing wave equation of guided wave in contact wire can be finally obtained.

The final governing wave equation is an eigensystem, and the solution of the eigensystem reveals the eigenvalue ξ corresponds to the wavenumber of the guided wave modes at a certain frequency ω satisfying the resonant condition of this contact wire. The frequency ω is always positive real, and the wavenumber ξ can be either complex or real. When ξ_m is a real number, the mth mode is a propagation mode, and for complex ξ_m, the mth mode is an evanescent mode. Then, the phase velocity c_m at the frequency ω for the mth mode is given by $c_m = \omega/\xi_m$. The group velocity accuracy is sensitive to the (ξ, ω) solutions. Therefore, the group velocity can be calculated for each individual (ξ, ω) solution point of the dispersion relations at a time without any contribution from adjacent points. Finally, the phase and group velocity dispersion curves for TCG-110 contact wire can be obtained.

Fig. 3 shows the phase and group velocity dispersion curves for contact wire with longitudinal wave velocity $c_L = 4422$ m/s and transverse wave velocity $c_T = 2247$ m/s. It should be noted that there is no previous literature on the study of guided waves in contact wire; thus, the wave mode numbering system proposed in [27] and [28] is used to name the guided wave modes in the contact wire studied in this article. The three fundamental modes with no cutoff frequencies are named $M1$, $M2$, and $M3$, respectively, as shown in Fig. 3. Higher-order modes starting from $M4$ are numbered based on their cutoff frequencies.

As demonstrated in Fig. 3, in the low-frequency range below 100 kHz, three fundamental propagating modes exist, and higher-order modes appear with the increase in frequency. The $M2$ mode has no dispersive behavior and propagates at a constant velocity, and its velocity is the same as that of

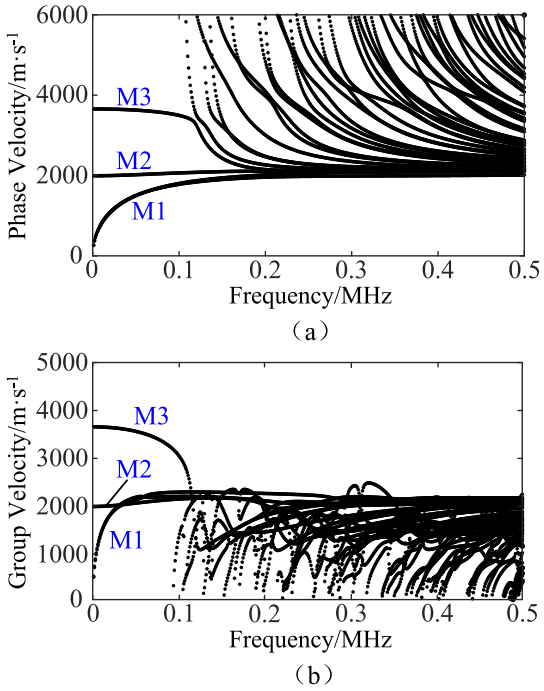

Fig. 3. Dispersion curves for TCG-110 contact wire. (a) Phase velocity. (b) Group velocity.

transverse wave. In addition, the other modes are with obvious dispersive behavior. There is a less-dispersive region in the low frequency where the $M1$ and $M3$ modes with less-dispersive behavior propagate at almost constant velocities, which is usually considered as the nondispersion region.

B. Mode Analysis and Selection

Theoretical dispersion curves for contact wire show that there are a large number of propagation modes with close group and phase velocities. However, these modes are usually useless in practical applications. Because of the existence of undesired modes, it is very difficult to generate an ideal single mode. The measured signal usually contains multiple modes, which increases the complexity of the detection signals. Moreover, the shape of a propagating wave changes with distance along the propagation path due to the dispersive nature of guided wave, which leads to signal-to-noise ratio problems and makes the measured signal difficult to interpret [29], [30]. Therefore, it is necessary to select an ideal mode and an appropriate frequency of the test to obtain a simple measured signal, which contains complete detection information and is easy to interpret.

The dispersion curves in Fig. 3 show that in the low-frequency range below 100 kHz, where frequency being below the cutoff frequencies of higher-order modes, only three propagating modes exist. Also, within this frequency range, the $M1$ and $M3$ modes have a less-dispersive region. To select an appropriate mode for damage identification, it is necessary to know the mode shapes to design an appropriate wave excitation/detection approach. Therefore, the displacement fields of three representative modes ($M1$, $M2$, and $M3$) are

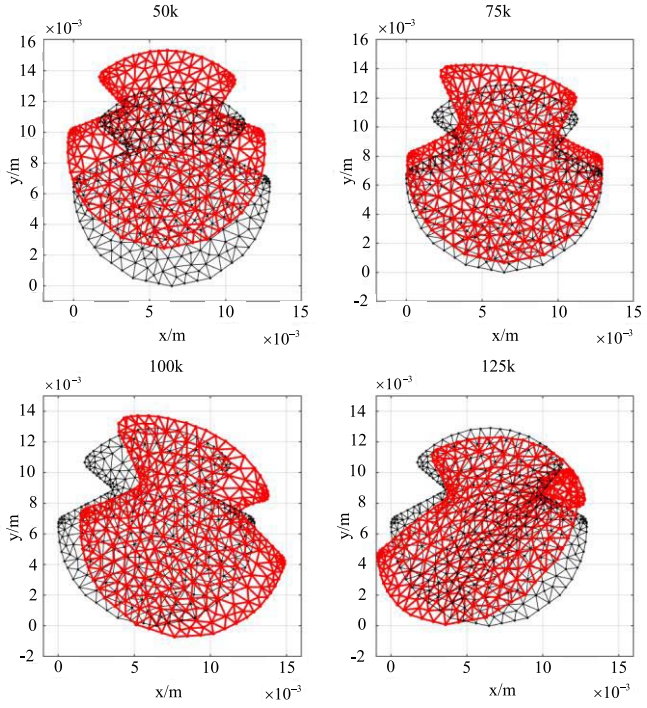

Fig. 4. Cross-sectional displacement diagram of the $M1$ mode at different frequencies.

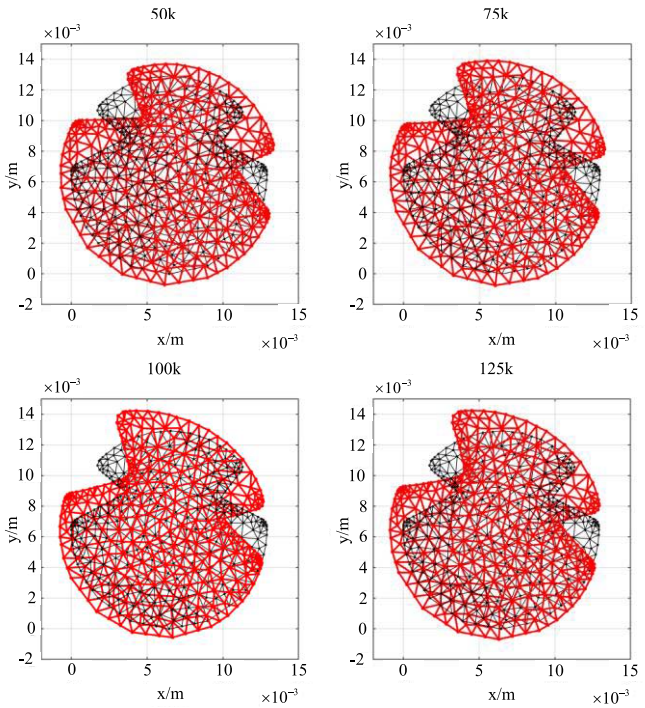

Fig. 5. Cross-sectional displacement diagram of the $M2$ mode at different frequencies.

discussed in detail within the frequency range of 50–125 kHz in this part.

The wave structures of the $M1$ mode at different frequencies are shown in Fig. 4, and wave structures at both maximum displacement and zero displacement (original cross section) are shown to provide a reference. As can be seen from Fig. 4, the form changes of contact wire cross section increase with higher frequency, and the displacement of wave is the largest at a frequency of 125 kHz due to the larger inertia of the corners. These wave structures are nonsymmetric about the centerline of cross section. The mode shape of $M1$ is similar to that of the flexural type modes in pipeline, where the flexural modes vibrate the entire cross section in three directions.

The wave structures in Fig. 5 show that the $M2$ mode at different frequencies has similar wave structures, and the particle motion on the cross section is predominantly circumferential. Compared with the original cross section (zero displacement), the wave structures at a frequency of 50 and 75 kHz are without any changes, while the wave structures at a frequency of 100 and 125 kHz are with slight deformations. These wave structures, however, can still be regarded as symmetrical about the centerline of cross section. Also, the dispersion characteristics of the $M2$ mode (shown in Fig. 3) are similar to the $T(0,1)$ mode in pipeline. Therefore, the $M2$ mode in contact wire can be considered as the torsional-like mode.

As demonstrated in Fig. 6, the wave structures of the $M3$ mode at the frequencies of 50, 75, and 100 kHz are symmetrical about the centerline of cross section and with no or little form deformation. These wave structures vibrate in a plate-like region with a uniform displacement in the longitudinal direction, and the particle motion on the cross

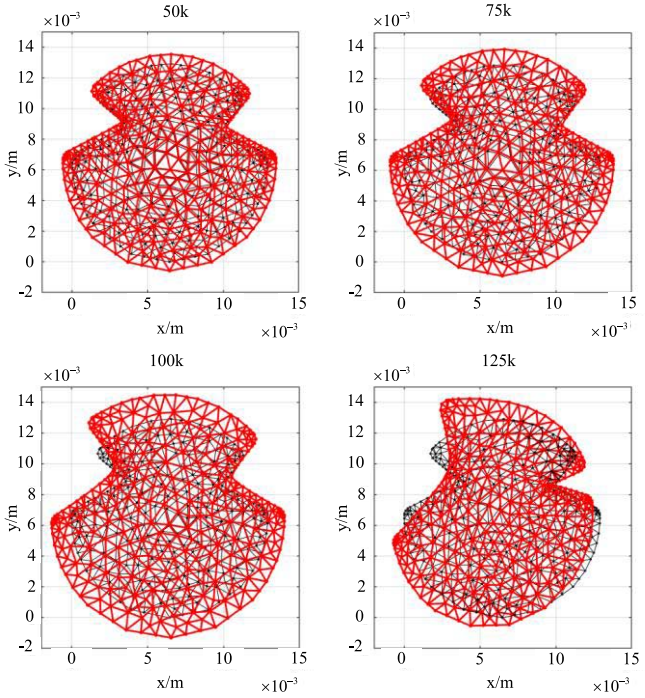

Fig. 6. Cross-sectional displacement diagram of the $M3$ mode at different frequencies.

section is predominantly longitudinal. The form of contact wire cross section at a frequency of 125 kHz is seriously damaged, and the wave structure is nonsymmetric. Obviously, the $M3$ mode is a longitudinal-like mode, and it is similar to the longitudinal mode in pipeline.

The dispersion curves of Fig. 3 show that the $M3$ mode in the frequency range of 50–100 kHz is the fastest mode and

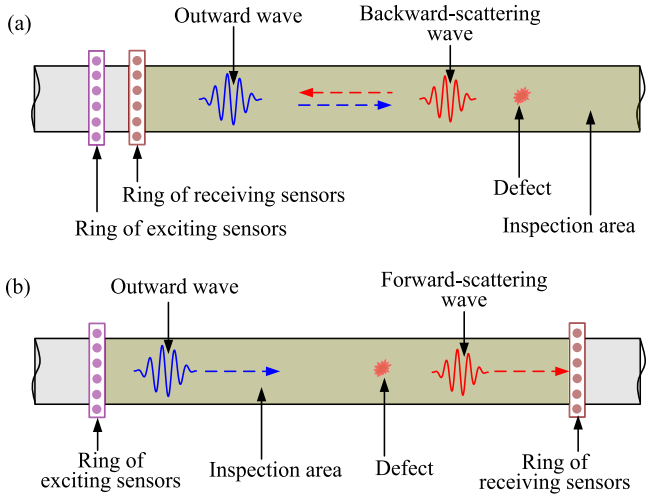

Fig. 7. Configurations used in guided wave inspection. (a) Pulse echo. (b) Pitch catch.

is also practically nondispersive. To simplify the interpretation of the measured signals, it is essential to excite a single guided wave mode in a nondispersive or less-dispersive frequency region [31], [32], because dispersion will lead to the change of the shape and amplitude of the signal as it travels. Meanwhile, selecting the fastest guided wave mode will help to separate the signals of interest from the other measured signals in time domain [31], [32]. The mode analysis results show that the mode shape of $M3$ is similar to the longitudinal mode in pipeline, and the particle motion on the cross section is predominantly longitudinal. It is very suitable for detecting internal or surface defects of contact wire. Therefore, the $M3$ mode is ideal for the proposed application, and it is found that satisfactory results can be obtained by testing at the frequencies around 75 kHz.

III. Experiments Validation

A. Experimental Scheme

There are usually two basic configurations in guide wave inspection, "pulse echo" [33], [34] and "pitch catch" [35], [36], as shown in Fig. 7(a) and (b), respectively. In a pulse-echo configuration where exciting sensors and receiving sensors are placed on the same side of the inspection area, a diagnostic guided wave signal is transmitted from the exciting sensors and travels through the inspection area, and the backscattering wave (signals reflected from the structural damage) is received by the receiving sensors. In a pitch-catch configuration, the guided wave signal is activated by an exciting sensor to propagate through the inspection area while the forward-scattering wave (signals propagate through the inspection area) is captured by receiving sensors on the other side of the area.

The main difference between two configurations is that the sensitivity of pulse-echo configuration is controlled by the amplitude of backscattering wave signals reflected from the structural damage, whereas the sensitivity of pitch-catch configuration is governed by the amplitude of forward-scattering wave signals propagate through the inspection area [37].

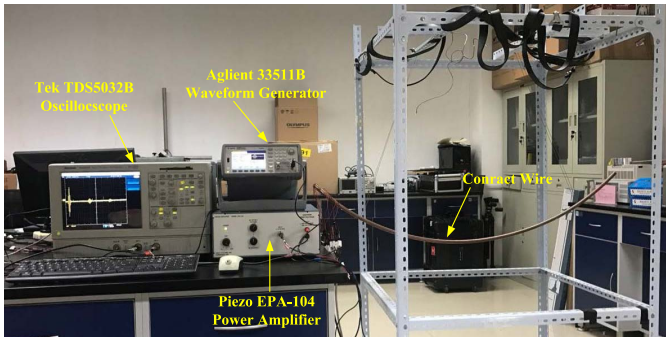

Fig. 8. Experimental apparatus.

Compared with backscattering wave signal, forward-scattering wave signal cannot be used to locate the defect unless a network of transducers is employed to provide more forward-scattering wave signals. In this article, the pulse-echo configuration is employed to identify the defects in contact wire.

B. Experimental Apparatus

The experimental apparatus employed in this article is shown in Fig. 8. First, excitation signal is generated by the Agilent 33511B arbitrary waveform generator; then, the excitation signal is amplified by PIEZO EPA-104 linear power amplifier in a suitable voltage range, and Tek TDS5032B digital oscilloscope is used to capture measured signals. Meanwhile, two ring arrays of piezoelectric elements are placed around the circumference to excite and receive signals, respectively.

To verify the effectiveness of guided wave contact wire detection, two cases are discussed in this article. One is defectless and labeled as Case 1. The other one is that with four artificial defects in different positions around the circumference and labeled as Case 2. The position and depth of different defects are shown in Fig. 9.

C. Experimental Results

According to the pulse-echo principle, at a location where there is a defect in contact wire, an echo is generated in the received signal, correspondingly. Based on the difference in the time of flight between the defect and incident wave, and the predicted speed of the selected mode at a particular frequency, the distance of defect in relation to the position of the transducer array can be calculated. The testing result of Case 1 is shown in Fig. 10(a), and there are no other reflected echoes in the measured signal except two obvious pluses, which are incident pulse and end echo, respectively. This is consistent with the theoretical analysis, because Case 1 is defectless.

The testing result of Case 2 is shown in Fig. 10(b), theoretically, and there should be four reflected echoes in the measured signal that correspond to four different defects in Case 2. In fact, only one obvious echo exists in Fig. 10(b) except the incident pulse and end echo; this is mainly because the size of cracks A and B is relatively small, leading to the amplitude of reflected echoes of cracks A and B that are too

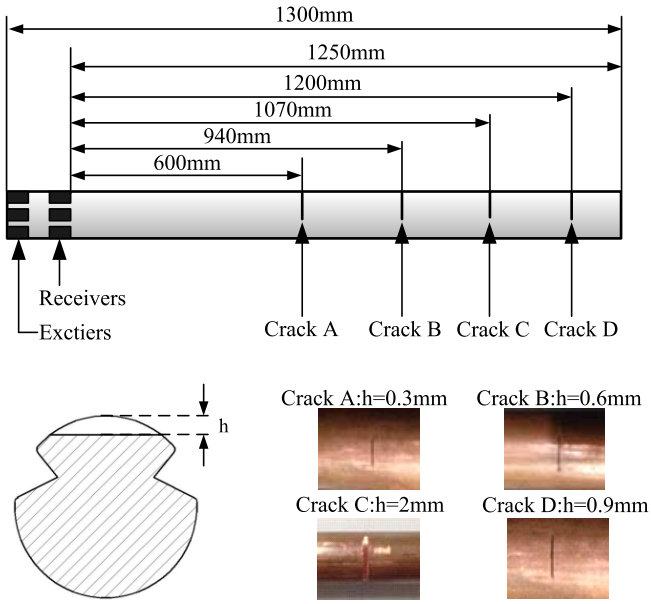

Fig. 9. Position and depth of defects in contact wire.

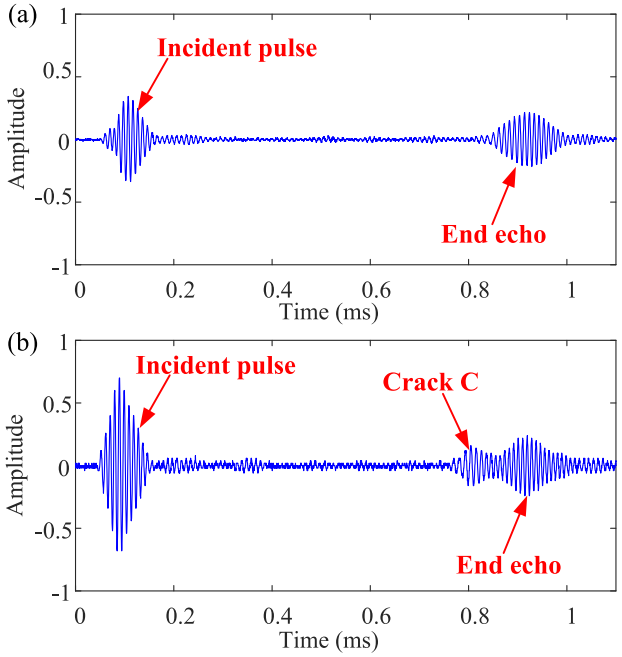

Fig. 10. Testing results of contact wire inspection. (a) Case 1. (b) Case 2.

small to be identified. In addition, the axial distance between crack D and end surface is shorter than half-bandwidth of the excitation signal, resulting in the reflected echo of crack D that is overlapped with end echo and form a single echo. Obviously, useful position information of defects cannot be extracted directly from the original signal without further processing. Therefore, it is necessary to employ an effective method to improve the time resolution of guided wave signal.

IV. Sparse Deconvolution Method

According to the pulse-echo principle, the measured signal obtained from guided wave inspection can be mathematically

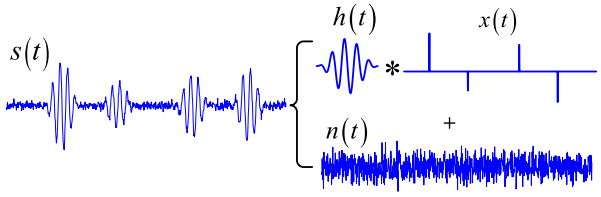

Fig. 11. Convolution model of guided wave signal.

modeled as the convolution of the incident pulse and reflection sequence

$$s(t) = h(t) * x(t) + n(t) \tag{1}$$

where $s(t)$ is the measured signal, $h(t)$ is the incident pulse, $x(t)$ is the reflection sequence, and $n(t)$ is the noise, and the symbol $*$ denotes the convolution operation, as illustrated in Fig. 11.

The purpose of deconvolution is to recover the reflection sequence $x(t)$ from the measured signal $s(t)$, because the reflection sequence $x(t)$ contains the same information as the measured signal $s(t)$, and the resolution of $x(t)$ is much higher than $s(t)$. Deconvolution is an inverse problem, and it is better to formulate the convolution model in (1) as discrete notation

$$s = Hx + n \tag{2}$$

where H is the convolution matrix, and H is a Toeplitz matrix whose columns are the incident pulse $h(t)$.

It is well known that the problem of recovering the reflection sequence $x(t)$ from measured signal $s(t)$ is an ill-posed problem; thus, this inverse problem cannot be satisfactorily solved unless some prior information is adopted. For guided wave inspection, the occurrence of an echo in the measured signal $s(t)$ generates a value in reflection sequence $x(t)$ correspondingly, and the other values in $x(t)$ will be zeroes. This implies that the reflection sequence $x(t)$ will be sparse, i.e., has the fewest nonzero values [34]. This is a useful information that needs to be exploited for deconvolution. Usually, the l_1-norm is used to induce sparsity. In this case, the solution of problem (2) can be found by an optimization problem

$$\arg\min_x \frac{1}{2}\|s - Hx\|_2^2 + \lambda\|x\|_1 \tag{3}$$

where $\|x\|_1$ is the l_1-norm of the solution and is defined as $\|x\|_1 = \sum_{i=1}^{m} |x_i|$, and λ is the regularization parameter. Problem (3) is also known as the basis pursuit denoising (BPD) problem [38], [39], which can be solved only by running the iterative numerical algorithm. A good algorithm is one with high computational efficiency and fast convergence. Some different algorithms have been developed by different groups for solving the BPD problems [40]–[42]. Split variable augmented Lagtangrian shrinkage algorithm (SALSA) is an effective algorithm to solve the BPD problem, and the good convergence, in practice, has been proven in [43], [44]. Therefore, the SALSA algorithm is employed to solve the deconvolution problem in this article.

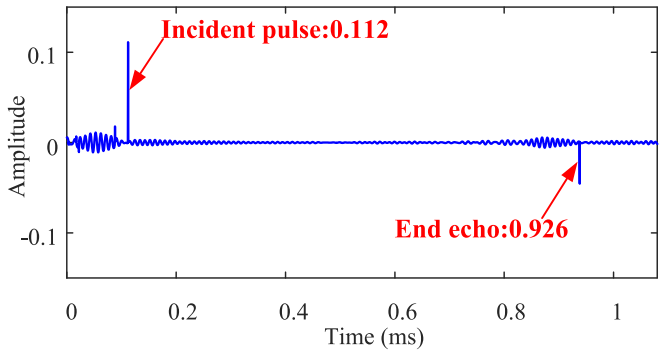

Fig. 12. Sparse deconvolution result of Case 1.

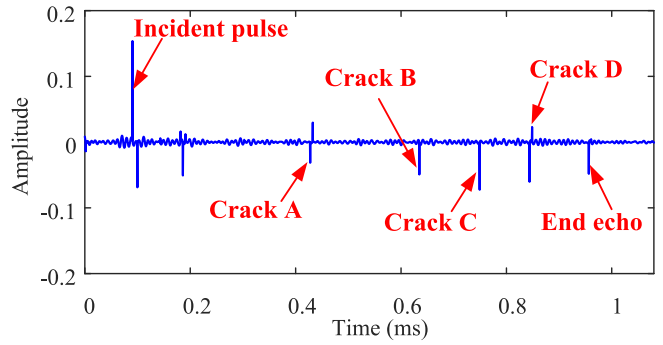

Fig. 13. Sparse deconvolution result of Case 2.

V. Analysis Results

A. Case 1

The measured signal of Case 1 [as shown in Fig. 10(a)] is processed by the sparse deconvolution method, and the result is shown in Fig. 12. There are only two obvious spikes in the recovered reflection sequence correspond to the incident pulse and end echo in the original testing signal, respectively. This is in accordance with the previous theoretical analysis and experimental result. As can be seen from Fig. 12, time difference between the incident pulse and end echo is 0.814 ms, and the distance from the end face to the receivers is 1.25 m; then, the group velocity of the $M3$ mode is 3071.3 m/s. In the theoretical calculation of dispersion curves (as shown in Fig. 3), the group velocity of the $M3$ mode is 3209 m/s at a frequency of 75 kHz. Considering the influence of background noise and measurement error, it is considered that the calculation result of group velocity of the $M3$ mode is in agreement with the theoretical value.

B. Case 2

The deconvolution result of Case 2 is shown in Fig. 13. Compared with the original testing signal of Case 2 [as shown in Fig. 10(b)], the resolution of sparse deconvolution result is significantly improved. The reflected echoes of cracks A and B, which drown in noise, are restored; meanwhile, the overlapping echoes of crack D and end echo are well distinguished. Meanwhile, there are bilateral peaks around cracks A and D, which is caused by the dispersion characteristic of guided wave. The sparse deconvolution algorithm is essentially a regularization method based on $L1$-norm, which is highly sensitive to the changes in the profile of waveform. Due to the dispersion property of guided wave, the incident pulse observed by the received sensors usually changes considerably while it propagates along the structure under test [31], [32]. Therefore, the bilateral peaks around cracks A and D are the artifacts resulting from the alteration in wavelet profile, which is caused by the dispersion characteristic of guided wave.

TABLE II
Calculation Results of the Position of Cracks

—	Response Time (ms)	Time Difference (ms)	Actual Position (mm)	Detection Result (mm)	Error (%)
Incident Pulse	0.0904	—	—	—	—
Crack A	0.4424	0.352	600	564.8	5.87
Crack B	0.6648	0.5744	940	921.6	1.96
Crack C	0.7512	0.6608	1070	1060.3	0.91
Crack D	0.844	0.7536	1200	1209.2	0.77

The detection information, which is hard to be extracted from the original signal, can be easily extracted from the deconvolution result. According to the extracted time information and the theoretical group velocity of $M3$, the positon of the cracks can be calculated, which is shown in Table II. As can be seen from Table II, the range of measurement error of crack position is 0.77%–5.87%. In addition to the larger measurement error of crack A, the relative errors of other cracks are acceptable. The major reason for the large measurement error of crack A is that the size of crack A is the smallest of all the cracks, and this leads to the reflected echo of crack A to be relatively weak. So, the measurement result of crack A is more easily influenced by noise than other cracks.

VI. Conclusion

A novel defect detection method for contact wire based on ultrasonic guide wave has been described in this article. The SAFE method was employed to study the propagation characteristics of guided wave in contact wire. The phase and group velocity dispersive curves for contact wire have been shown that there were three propagation modes existing in the low frequency range below 100 kHz, and higher-order modes appeared as an increase in the frequency. The $M1$ and $M3$ modes were with obvious dispersive behavior, while the $M2$ mode was nondispersive.

The displacement fields of three domain modes ($M1$, $M2$, and $M3$ modes) were discussed in detail within the frequency range of 50–125 kHz. Those domain modes can be considered as the flexural-like, torsional-like, and longitudinal-like modes in pipeline, respectively. It has been shown that the $M3$ mode in the frequency range of 50–100 kHz was an ideal mode for the proposed application.

Two basic configurations used in guided wave inspection were discussed, and the pulse echo was finally employed to identify the defects in contact wire. The experimental results

were shown shat the proposed method could effectively detect the defects in contact wire. To extract the useful position information of defects, the sparse deconvolution method was studied based on the convolution model of guided wave signal and sparse theory. It was found that the time resolution of guided wave signal was significantly improved by the sparse deconvolution method, because the echoes overlapping and drown problems in original signal were well solved by the sparse deconvolution method.

REFERENCES

[1] H. Hofler, M. Dambacher, N. Dimopoulos, and V. Jetter, "Monitoring and inspecting overhead wires and supporting structures," in *Proc. IEEE Intell. Vehicles Symp.*, Jun. 2004, pp. 512–517.

[2] A. Daadbin and J. Rosinski, "Development, testing and implementation of the pantograph damage assessment system (PANDAS)," *WIT Trans. Built Environ.*, vol. 114, pp. 573–578, Jul. 2010.

[3] S. Liu, Q. Wang, and Y. Luo, "A review of applications of visual inspection technology based on image processing in the railway industry," *Transp. Saf. Environ.*, vol. 1, no. 3, pp. 185–204, Dec. 2019.

[4] S. Borromeo, J. L. Aparicio, and P. M. Martinez, "MEDES: Contact wire wear measuring system used by the Spanish national railway (RENFE)," *Proc. Inst. Mech. Eng., F, J. Rail Rapid Transit*, vol. 217, no. 3, pp. 167–175, May 2003.

[5] F. Q. Yuan and J. M. Lu, "Data-driven model development using support vector machine for railway overhead contact wire maintenance," in *Proc. IEEE Int. Conf. Ind. Eng. Eng. Manage. (IEEM)*, Dec. 2015, pp. 78–82.

[6] I. Aydin, M. Karakose, and E. Akin, "A new contactless fault diagnosis approach for pantograph-catenary system using pattern recognition and image processing methods," *Adv. Elect. Comput. Eng.*, vol. 14, no. 3, pp. 79–89, 2014.

[7] L. Aydin, "A new approach based on firefly algorithm for vision-based railway overhead inspection system," *Measurement*, vol. 74, pp. 43–55, Oct. 2015.

[8] S. Borromeo and J. L. Aparicio, "Automatic systems for wear measurement of contact wire in railways," in *Proc. IEEE 28th Annu. Conf. Ind. Electron. Soc. (IECON)*, Nov. 2002, pp. 2700–2705.

[9] J. L. Rose, "A baseline and vision of ultrasonic guided wave inspection potential," *J. Pressure Vessel Technol.*, vol. 124, no. 3, pp. 273–282, Aug. 2002, doi: 10.1115/1.1491272.

[10] D. Zhang, Z. Zhou, J. Sun, E. Zhang, Y. Yang, and M. Zhao, "A magnetostrictive guided-wave nondestructive testing method with multifrequency excitation pulse signal," *IEEE Trans. Instrum. Meas.*, vol. 63, no. 12, pp. 3058–3066, Dec. 2014.

[11] J. L. Rose, "Ultrasonic guided waves in structural health monitoring," *Key Eng. Mater.*, vol. 270, no. 1, pp. 14–21, 2004.

[12] B. Zhang, X. Hong, and Y. Liu, "Deep convolutional neural network probability imaging for plate structural health monitoring using guided waves," *IEEE Trans. Instrum. Meas.*, vol. 70, pp. 1–10, 2021.

[13] L. Zeng, Z. Luo, J. Lin, and J. Hua, "Excitation of Lamb waves over a large frequency-thickness product range for corrosion detection," *Smart Mater. Struct.*, vol. 26, no. 9, Sep. 2017, Art. no. 095012.

[14] C. Xu, Z. Yang, B. Qiao, and X. Chen, "A parameter estimation based sparse representation approach for mode separation and dispersion compensation of Lamb waves in isotropic plate," *Smart Mater. Struct.*, vol. 29, no. 3, Mar. 2020, Art. no. 035020.

[15] W. Gao, D. Zhang, E. Zhang, and X. Yan, "Noncontact magnetostrictive torsional guided wave sensors for small-diameter pipes," *IEEE Trans. Instrum. Meas.*, vol. 70, pp. 1–9, 2021.

[16] Z. Wang, S. Huang, S. Wang, S. Zhuang, Q. Wang, and W. Zhao, "Compressed sensing method for health monitoring of pipelines based on guided wave inspection," *IEEE Trans. Instrum. Meas.*, vol. 69, no. 7, pp. 4722–4731, Jul. 2020.

[17] S. S. Bang, Y. H. Lee, and Y.-J. Shin, "Defect detection in pipelines via guided wave-based time–frequency-domain reflectometry," *IEEE Trans. Instrum. Meas.*, vol. 70, pp. 1–11, 2021.

[18] J. J. da Silva, M. G. Wanzeller, P. de Almeida Farias, and J. S. da Rocha Neto, "Development of circuits for excitation and reception in ultrasonic transducers for generation of guided waves in hollow cylinders for fouling detection," *IEEE Trans. Instrum. Meas.*, vol. 57, no. 6, pp. 1149–1153, Jun. 2008.

[19] F. Gao, L. Zeng, J. Lin, and Y. Shao, "Damage assessment in composite laminates via broadband Lamb wave," *Ultrasonics*, vol. 86, pp. 49–58, May 2018.

[20] Y. Hu, F. Cui, F. Li, X. Tu, and L. Zeng, "Sparse wavenumber analysis of guided wave based on hybrid lasso regression in composite laminates," *Struct. Health Monitor.*, Jul. 2021, Art. no. 147592172110321, doi: 10.1177/14759217211032118.

[21] C.-B. Xu, Z.-B. Yang, Z. Zhai, B.-J. Qiao, S.-H. Tian, and X.-F. Chen, "A weighted sparse reconstruction-based ultrasonic guided wave anomaly imaging method for composite laminates," *Compos. Struct.*, vol. 209, pp. 233–241, Feb. 2019.

[22] Y. Liu, X. Hong, and B. Zhang, "A novel velocity anisotropy probability imaging method using ultrasonic guided waves for composite plates," *Measurement*, vol. 166, Dec. 2020, Art. no. 108087.

[23] T. Hayashi, W.-J. Song, and J. L. Rose, "Guided wave dispersion curves for a bar with an arbitrary cross-section, a rod and rail example," *Ultrasonics*, vol. 41, pp. 175–183, May 2003.

[24] T. Hayashi, C. Tamayama, and M. Murase, "Wave structure analysis of guided waves in a bar with an arbitrary cross-section," *Ultrasonics*, vol. 44, no. 1, p. 17, 2006.

[25] I. Bartoli, A. Marzani, F. L. D. Scalea, and E. Viola, "Modeling wave propagation in damped waveguides of arbitrary cross-section," *J. Sound Vibrat.*, vol. 295, no. 3, pp. 685–707, 2006.

[26] A. Marzani, E. Viola, I. Bartoli, F. L. di Scalea, and P. Rizzo, "A semi-analytical finite element formulation for modeling stress wave propagation in axisymmetric damped waveguides," *J. Sound Vibrat.*, vol. 318, no. 3, pp. 488–505, Dec. 2008.

[27] H. Gao, *Ultrasonic Guided Wave Mechanics for Composite Material Structural Health Monitoring*. State College, PA, USA: Pennsylvania State Univ., 2007.

[28] J. L. Rose, *Ultrasonic Guided Waves in Solid Media*. Cambridge, U.K.: Cambridge Univ. Press, 2014.

[29] P. D. Wilcox, M. J. S. Lowe, and P. Cawley, "The effect of dispersion on long-range inspection using ultrasonic guided waves," *NDT E Int.*, vol. 34, no. 1, pp. 1–9, 2001.

[30] C.-B. Xu, Z.-B. Yang, X.-F. Chen, S.-H. Tian, and Y. Xie, "A guided wave dispersion compensation method based on compressed sensing," *Mech. Syst. Signal Process.*, vol. 103, pp. 89–104, Mar. 2018.

[31] M. J. S. Lowe, D. N. Alleyne, and P. Cawley, "Defect detection in pipes using guided waves," *Ultrasonics*, vol. 36, nos. 1–5, pp. 147–154, 1998.

[32] P. D. Wilcox *et al.*, "Mode and transducer selection for long range Lamb wave inspection," *Key Eng. Mater.*, vols. 167–168, no. 8, pp. 152–161, 1999.

[33] A. Raghavan and C. E. S. Cesnik, "Effects of elevated temperature on guided-wave structural health monitoring," *J. Intell. Mater. Syst. Struct.*, vol. 19, no. 12, pp. 1383–1398, 2008.

[34] A. C. Raghavan and C. E. S. Cesnik, "Review of guided-wave structural health monitoring," *Shock Vib. Dig.*, vol. 39, no. 2, pp. 91–114, 2007.

[35] K. Harri, P. Guillaume, and S. Vanlanduit, "On-line damage detection on a wing panel using transmission of multisine ultrasonic waves," *NDT E Int.*, vol. 41, no. 4, pp. 312–317, Jun. 2008.

[36] J.-B. Ihn and F.-K. Chang, "Pitch-catch active sensing methods in structural health monitoring for aircraft structures," *Struct. Health Monitor.*, vol. 7, no. 1, pp. 5–19, 2008.

[37] Z. Su and L. Ye, *Identification of Damage Using Lamb Waves*. London, U.K.: Springer, 2009, pp. 195–254.

[38] S. S. Chen, D. L. Donoho, and M. A. Saunders, "Atomic decomposition by basis pursuit," *SIAM J. Sci. Comput.*, vol. 20, no. 1, pp. 33–61, Jul. 1998.

[39] B. Yang, R. Liu, and X. Chen, "Sparse time-frequency representation for incipient fault diagnosis of wind turbine drive train," *IEEE Trans. Instrum. Meas.*, vol. 67, no. 11, pp. 2616–2627, May 2018.

[40] I. Daubechies, M. Defrise, and C. De Mol, "An iterative thresholding algorithm for linear inverse problems with a sparsity constraint," *Commun. Pure Appl. Math.*, vol. 57, no. 11, pp. 1413–1457, Nov. 2004.

[41] J. M. Bioucas-Dias and M. A. T. Figueiredo, "A new TwIST: Two-step iterative shrinkage/thresholding algorithms for image restoration," *IEEE Trans. Image Process.*, vol. 16, no. 12, pp. 2992–3004, Dec. 2007.

[42] M. V. Afonso, J.-M. Bioucas-Dias, and M. A. T. Figueiredo, "Fast image recovery using variable splitting and constrained optimization," *IEEE Trans. Image Process.*, vol. 19, no. 9, pp. 2345–2356, Sep. 2010.

[43] Y. Chang, Y. Zi, J. Zhao, Z. Yang, W. He, and H. Sun, "An adaptive sparse deconvolution method for distinguishing the overlapping echoes of ultrasonic guided waves for pipeline crack inspection," *Meas. Sci. Technol.*, vol. 28, no. 3, Mar. 2017, Art. no. 035002.

[44] W. He, Y. Ding, Y. Zi, and I. W. Selesnick, "Sparsity-based algorithm for detecting faults in rotating machines," *Mech. Syst. Signal Process.*, vols. 72–73, pp. 46–64, May 2016.

Yong Chang received the B.Eng. and M.Eng. degrees in mechanical engineering from the School of Mechanical and Power Engineering, Henan Polytechnic University, Jiaozuo, China, in 2009 and 2012, respectively, and the Ph.D degree in mechanical engineering from Xi'an Jiaotong University, Xi'an, China, in 2018.

He is currently an Associate Professor with the School of Electromechanical Engineering, Henan University of Technology, Zhengzhou, China. His current research interests include mechanical fault prognostics, health management, and ultrasonic nondestructive testing.

Nana Li received the B.Eng. degree in mechanical engineering from the School of Mechanical and Power Engineering, Henan Polytechnic University, Jiaozuo, China, in 2012, and the M.Eng. degree in mechanical engineering from Northwestern Polytechnical University, Xi'an, China, in 2015.

She is currently an Engineer with the Zhengzhou Research Institute of Mechanical Engineering, Zhengzhou, China. Her current research interests include mechanical fault prognostics, health management, and signal processing.

Jiyuan Zhao received the B.S. and M.S. degrees in mechanical manufacturing and automation and the Ph.D. degree in manufacturing and automation from Xi'an Jiaotong University, Xi'an, China, in 1991, 1994, and 1997, respectively.

From 1997 to 2009, he was an Engineer, a Senior Engineer, the Chief Engineer, and a Project Manager in the field of railway automation with Siemens, Beijing, China, a transportation system, and a member of the Institution of Railway Signaling Engineers, London, U.K. He is currently a Professor with Xi'an Jiaotong University. His current research interests include 3-D printing, high-end equipment condition monitoring and fault diagnosis, and nondestructive testing (NDT), especially in laser ultrasonic and industrial X-ray current transformer (CT).

Yu Wang (Senior Member, IEEE) received the B.Eng. degree in mechanical design and manufacturing automation from the Xi'an University of Technology, Xi'an, China, in 2005, the M.Eng. degree in manufacturing engineering and automation from Xi'an Jiaotong University, Xi'an, in 2008, and the Ph.D. degree in systems engineering and engineering management from the City University of Hong Kong, Hong Kong, in 2014.

He is currently an Associate Professor with the School of Mechanical Engineering, Xi'an Jiaotong University. His current research interests include reliability assessment, fault prognostics, and health management.

Zhe Yang received the B.E. degree in measurement and control and instrument and the M.Sc. degree in mechanical engineering from Xi'an Jiaotong University, Xi'an, China, in 2012 and 2015, respectively, and the Ph.D. degree in mechanical engineering from the Politecnico di Milano, Milan, Italy, in 2020.

He is currently a Post-Doctoral Fellow with Xi'an Jiaotong University and the Dongguan University of Technology, Dongguan, China. His research interests include the development of methods and techniques for prognostics and health management of industrial components.